Title
Three-Dimensional Turbulent Vortex Shedding From a Surface-Mounted Square Cylinder: Predictions With Large-Eddy Simulations and URANS

Journal
Journal of Fluids Engineering, 136(6)

ISSN
0098-2202

Authors
Younis, BA
Abrishamchi, A

Publication Date
2014-06-01

DOI
10.1115/1.4025254

Peer reviewed

Three-Dimensional Turbulent Vortex Shedding From a Surface-Mounted Square Cylinder: Predictions With Large-Eddy Simulations and URANS

B. A. Younis[1]
Department of Civil & Environmental Engineering,
University of California,
Davis, CA 95616
e-mail: bayounis@ucdavis.edu

A. Abrishamchi
Department of Civil & Environmental Engineering,
University of California,
Davis, CA 95616

The paper reports on the prediction of the turbulent flow field around a three-dimensional, surface mounted, square-sectioned cylinder at Reynolds numbers in the range 10^4–10^5. The effects of turbulence are accounted for in two different ways: by performing large-eddy simulations (LES) with a Smagorinsky model for the subgrid-scale motions and by solving the unsteady form of the Reynolds-averaged Navier–Stokes equations (URANS) together with a turbulence model to determine the resulting Reynolds stresses. The turbulence model used is a two-equation, eddy-viscosity closure that incorporates a term designed to account for the interactions between the organized mean-flow periodicity and the random turbulent motions. Comparisons with experimental data show that the two approaches yield results that are generally comparable and in good accord with the experimental data. The main conclusion of this work is that the URANS approach, which is considerably less demanding in terms of computer resources than LES, can reliably be used for the prediction of unsteady separated flows provided that the effects of organized mean-flow unsteadiness on the turbulence are properly accounted for in the turbulence model. [DOI: 10.1115/1.4025254]

Keywords: vortex shedding, URANS, LES, square cylinder, turbulence modeling

1 Introduction

The unsteady three-dimensional turbulent flow around a surface-mounted cylinder is of considerable interest to the fluids engineering community as evidenced by the large number of experimental and computational studies reported in recent years (e.g., Refs. [1–7]). At the high Reynolds numbers of engineering interest, the flow is fully turbulent and is characterized by the occurrence of vortex shedding that gives rise to oscillatory pressure forces at a well-defined frequency [8]. When the cylinder's aspect ratio is small, the flow around it, and the resulting surface-pressure distribution, become strongly three-dimensional leading to significant variations to occur along the cylinder's principal axis [9]. From an engineering standpoint, this three-dimensional behavior can be beneficial as it means that the unsteady forces that apply to the cylinder can become uncorrelated. Thus, while their frequency would be the same as the shedding frequency, their peaks would occur at different phases of the cycle depending on location along the cylinder. The eventuality of the correspondence between the frequency of the unsteady forces and the natural frequency of the cylinder is, thus, significantly reduced and with it the known hazards of structural resonance. It is, therefore, evident that the ability to accurately predict the occurrence of vortex shedding at high Reynolds number, as well as the three-dimensional nature of the flow and resulting forces, is critical to the design of tall, slender structures.

In this work, we assess the capabilities and limitations of two different modeling strategies that are frequently used for the prediction of the unsteady turbulent flows around three-dimensional structures at high Reynolds number. The first of these strategies is LES. The principles of this approach are well known. Briefly, the Navier–Stokes equations are averaged with respect to a predefined spatial filter. By solving the resulting filtered equations, all motions that occur with a spatial scale greater than that of the filter are computed directly, while those whose scale is smaller (the subscale motions) are not captured in the simulations and their effects must be introduced via a subgrid-scale model [10]. Previous relevant studies with LES include those of Lim et al. [5] for a flow around a cube in turbulent boundary layer over a rough surface, Krajnovic and Davidson [11] for a smooth-surface mounted cube at $Re = 10^4$, Sohankar [12] for a square-sectioned cylinder at $Re = 10^3$ and 5×10^6, and Oka and Ishihara [13] who used LES to investigate the effects of angle of attack on the aerodynamic coefficients and flow patterns around a square cylinder. The second approach is based on the solution of the URANS. Here, the averaging is done over a finite time interval (as distinct from the infinite time interval in the conventional Reynolds averaging) with the result that motions that have a greater time scale than that used in the averaging process are captured directly while the effects of motions having a shorter time scales are introduced via a turbulence closure. Previous work using URANS include that of Ramesh et al. [14]. The two approaches lead to quite different outcomes. In LES, the spatial filter size is usually set equal to the local dimensions of the computational cells that subdivide the solution domain. This has the undesirable effect of rendering the computed solutions dependent on the size of the computational mesh (Smith and Foster [15]). Thus, by changing the mesh

[1]Corresponding author.

Contributed by the Fluids Engineering Division of ASME for publication in the JOURNAL OF FLUIDS ENGINEERING. Manuscript received December 11, 2012; final manuscript received August 9, 2013; published online April 28, 2014. Assoc. Editor: Ye Zhou.

resolution, changes will also occur in the computed results thereby making it impossible to distinguish between numerical and modeling effects. It is for this reason that grid-independence of LES results is seldom demonstrated in practice (Pope [4]). On the other hand, in the limit of infinitesimally small mesh sizes, the contributions made by the subgrid scales model vanish entirely and with it the uncertainty associated with the use of a simple model to represent chaotic phenomenon. At present, however, the computer resources that are available for routine engineering computations of high Reynolds-number flows around full-scale structures are insufficient to entirely remove the need for a model for the subgrid motions. Consequently, the uncertainties associated with grid resolution effects cannot be entirely eliminated, or their importance quantified. In contrast, in the URANS approach, the computational mesh size does not enter into the formulation of the turbulence model and, hence, successive mesh refinement will eventually yield results that are grid independent and, thus, largely free of numerical discretization errors. The computational resources needed to attain grid-independent solutions are significantly less than with LES. The downside of the uncoupling of the turbulence model from the mesh size is that the inexorable increase in available computing power does not translate into reduction of the contribution made by the turbulence model, or of the modeling errors inherent in the various closure assumptions.

Clearly then, there are benefits and disadvantages to each of LES and URANS and the main purpose of this paper is to document these for the case of the surface-mounted square-sectioned cylinder at high Reynolds number. Of particular interest will be the performance of each approach with regards to capturing the expected occurrence of vortex shedding and of its consequences in terms of the pressure loading on the cylinder. While previous work has been reported in which either one of these approaches was used to predict the same flows, we are not aware of any that have compared LES with a URANS method that utilized a turbulence model that explicitly accounts for the effects of vortex shedding on the turbulence.

2 Mathematical Formulation

The predictions were obtained by solving the three-dimensional, time-dependent forms of the equations governing the conservation of mass and momentum. For incompressible flows, these equations are:
Continuity:

$$\frac{\partial \hat{U}_i}{\partial x_i} = 0 \tag{1}$$

Momentum:

$$\frac{\partial \hat{U}_i}{\partial t} + \frac{\partial \hat{U}_i \hat{U}_j}{\partial x_j} = \frac{\partial}{\partial x_j}\left(\nu \frac{\partial \hat{U}_i}{\partial x_j}\right) - \frac{1}{\rho}\frac{\partial \hat{p}}{\partial x_i} \tag{2}$$

In the above $\hat{U}_i$ is the instantaneous velocity vector, $\hat{p}$ is the static pressure, and ρ and ν are, respectively, the fluid's density and its kinematic viscosity. Cartesian–tensor notation is used wherein repeated indices imply summation.

For the large-eddy simulations, Eqs. (1) and (2) are averaged by integration over a filter width $\Delta\ (=(\delta x\ \delta y\ \delta z)^{1/3})$ to obtain

$$\frac{\partial \overline{U_i}}{\partial x_i} = 0 \tag{3}$$

$$\frac{\partial \overline{U_i}}{\partial t} + \frac{\partial \overline{U_i}\,\overline{U_j}}{\partial x_j} = \frac{\partial}{\partial x_j}\left(\nu \frac{\partial \overline{U_i}}{\partial x_j} - \tau_{ij}\right) - \frac{1}{\rho}\frac{\partial \overline{p}}{\partial x_i} \tag{4}$$

where $\overline{U}_i$ and $\bar{p}$ are the filtered velocity vector and pressure, respectively.

The quantity τ_{ij} in Eq. (4) is the anisotropic residual subgrid-scale stress tensor:

$$\tau_{ij} = \overline{U_i U_j} - \overline{U_i}\,\overline{U_j} \tag{5}$$

In most engineering applications of LES, this tensor is modeled after Smagorinsky who assumed it to be linearly proportional to the filtered strain-rate tensor $\overline{S}_{ij}$:

$$\tau_{ij} = -2\nu_t \overline{S}_{ij} - \frac{2}{3}\delta_{ij} k_r \tag{6}$$

where k_r is the residual kinetic energy and

$$\overline{S}_{ij} = \frac{1}{2}\left(\frac{\partial \overline{U}_i}{\partial x_j} + \frac{\partial \overline{U}_j}{\partial x_i}\right) \tag{7}$$

The quantity ν_t in Eq. (6) is the coefficient of proportionality in the Smagorinsky model that is usually modeled as a function of local parameters, specifically by analogy to the mixing-length hypothesis:

$$\nu_t = L_s^2 \overline{S} \tag{8}$$

$$= (C_s \Delta)^2 \overline{S} \tag{9}$$

In the above, L_s is the Smagorinsky lengthscale, which is assumed to be proportional to the filter width Δ, and $\overline{S}\ (=(2\overline{S}_{ij}\overline{S}_{ij})^{0.5})$ is the characteristic filtered rate of strain. C_s is the Smagorinsky constant, which is here assigned the value of 0.1 (e.g. Ref. [5]).

For the URANS calculations, the averaging of Eqs. (1) and (2) occurs over a time interval Δt:

$$\overline{U_i} = \frac{1}{\Delta t}\int_t^{t+\Delta t} \hat{U}_i dt \tag{10}$$

In the conventional Reynolds averaging approaches, the time interval Δt for integration is taken to be infinite. This would be appropriate for statistically stationary flows. In unsteady flows, the time interval is the same as the computational time step, thus, motions occurring at a time scale greater than the computational time step are captured directly, while those with a shorter time scale are averaged out and their effect is accounted for via a turbulence model. The equations that describe the URANS approach are now obtained by replacing the instantaneous variables in Eqs. (1) and (2) by the sum of computational time step averaged and fluctuating quantities and then by time averaging:

$$\frac{\partial \overline{U_i}}{\partial x_i} = 0 \tag{11}$$

$$\frac{\partial \overline{U_i}}{\partial t} + \frac{\overline{U_i}\,\overline{U_j}}{\partial x_j} = \frac{\partial}{\partial x_j}\left(\nu \frac{\partial \overline{U_i}}{\partial x_j} - \overline{u_i}\,\overline{u_j}\right) - \frac{1}{\rho}\frac{\partial \overline{p}}{\partial x_i} \tag{12}$$

where the overbars now denote computational time step averaged quantities and $\overline{u_i u_j}$ is the Reynolds stress tensor for which a turbulence model is required. In this study, a two–equation model of turbulence is used to determine the Reynolds stresses. At this level of closure, the Reynolds stresses are taken to be proportional to the local mean rates of strain $\overline{S}_{ij}$:

$$-\overline{u_i u_j} = 2\nu_t \overline{S}_{ij} - \frac{2}{3}\delta_{ij} k \tag{13}$$

where k is the turbulence kinetic energy, and $\overline{S}_{ij}$ is defined as in Eq. (7) but with the overbars taken to signify computational time step averaged quantities.

In the k-ϵ model used here, the eddy viscosity ν_t in Eq. (13) is obtained from

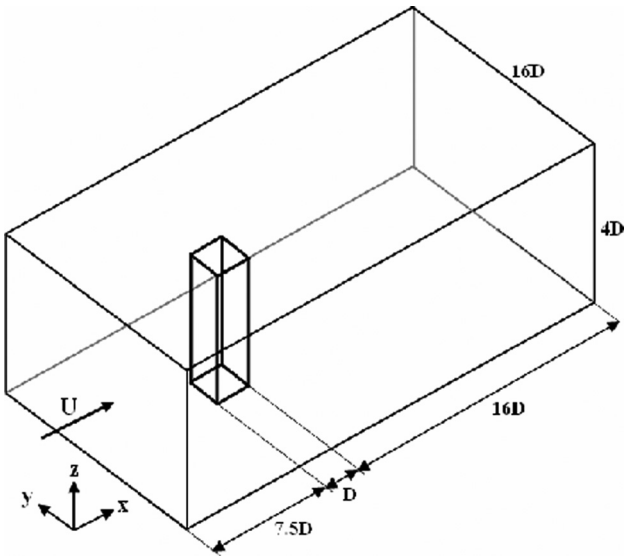

Fig. 1 Geometry, computational domain, and dimensions

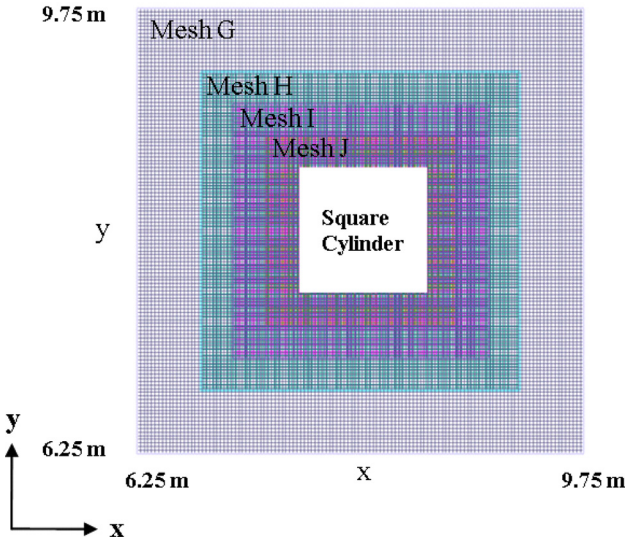

Fig. 2 Close-up of mesh in x-y plane

Table 1 Grid Convergence Index results for the modified k-ϵ model ($Re = 10^5$)

N_1	617,882
N_2	475,294
N_3	365,610
Φ	C_D
Φ_1	2.131
Φ_2	2.120
Φ_3	2.047
Φ_{ext}^{21}	2.133
e_{ext}^{21}	0.0915%
$\text{GCI}_{\text{fine}}^{21}$	0.11448%

$$\nu_t = C_\mu \frac{k^2}{\epsilon} \tag{14}$$

The turbulence kinetic energy k and its dissipation rate ϵ are determined from the solution of their own differential transport equations. These equations have the form

$$\frac{\partial k}{\partial t} + \overline{U_j}\frac{\partial k}{\partial x_j} = \frac{\partial}{\partial x_j}\left(\frac{\nu_t}{\sigma_k}\frac{\partial k}{\partial x_j}\right) + P_k - \epsilon \tag{15}$$

$$\frac{\partial \epsilon}{\partial t} + \overline{U_j}\frac{\partial \epsilon}{\partial x_j} = \frac{\partial}{\partial x_j}\left(\frac{\nu_t}{\sigma_\epsilon}\frac{\partial \epsilon}{\partial x_j}\right) + C_{\epsilon_1}\frac{\epsilon}{k}P_k - C_{\epsilon_2}\frac{\epsilon^2}{k} \tag{16}$$

where P_k is the rate of production of the turbulent kinetic energy:

$$P_k = -\overline{u_i u_j}\frac{\partial \overline{U_i}}{\partial x_j} \tag{17}$$

The model coefficients are assigned their standard values, viz., $(C_\mu, \sigma_k, \sigma_\epsilon, C_{\epsilon_1}, C_{\epsilon_2}) = (0.09, 1.0, 1.3, 1.45, 1.90)$.

The k-ϵ model in its standard form (Eqs. (14)–(16)) fails badly in capturing the main features of flows with vortex shedding. In particular, the model severely underestimates the magnitude of the fluctuations in the pressure field resulting in the underprediction of the root-mean-square values of the lift and drag coefficients. This defect of the standard model has been noted in a number of previous studies on isolated cylinders in uniform flow (e.g. Refs. [16,17]). As will be seen in Sec. 3, this model also fails

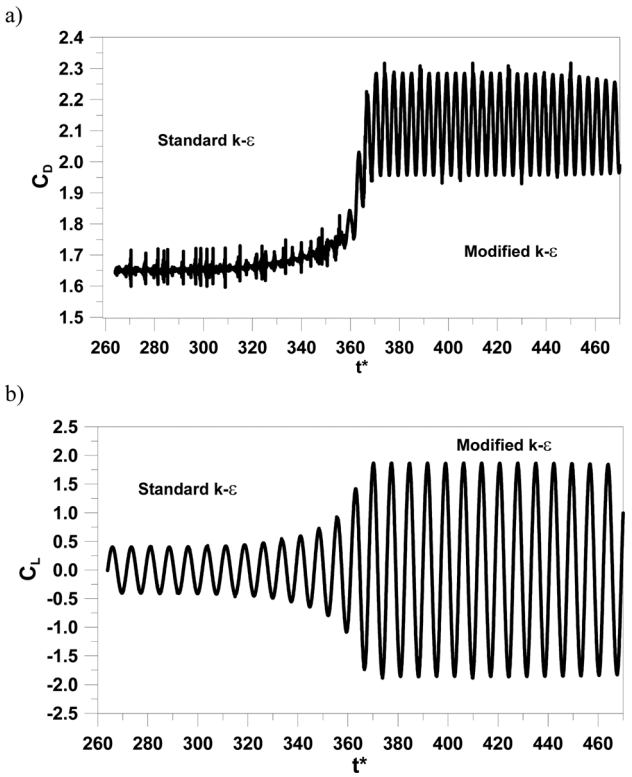

Fig. 3 Predicted drag (*a*) and lift (*b*) coefficients with standard and modified k-ϵ models ($Re = 10^5$)

in three-dimensional flows. Several reasons have been put forward in the literature to explain the causes. Younis and Zhou [18] have argued that this defect arises from the inability of this model to account for the interactions between the large-scale, organized, mean-flow unsteadiness due to vortex shedding and the small-scale random motions that characterize turbulence. The primary consequence of these interactions is the appearance of a peak in the turbulence-energy spectrum that represents direct transfer of energy from the mean flow into the turbulence. As expected, the frequency at which this peak of direct energy input occurs coincides exactly with the frequency of the vortex shedding (Durao et al. [19]). This direct transfer of energy at a discrete frequency is

Table 2 Predictions and measurements of mean flow parameters for a 3D square cylinder ($Re = 10^5$)

	St	C_D	C'_D	C'_L
Standard k-ε	0.122	1.652	0.011	0.321
Modified k-ε	0.146	2.120	0.114	1.301
LES (present)	0.125	2.229	0.280	1.188
LES [11] (Smagorinsky)	0.128	2.2	0.18	1.44
LES [11]	0.128	2.2	0.22	1.44
Experiments [22]	0.12	2.05	0.19	1.3

not accounted for in the standard model whose formulation is based on the assumption of spectral equilibrium. In order to account for this departure from equilibrium, it is necessary to reformulate the model on the basis of an energy spectrum function (E) that is different in form from that which is typically assumed for statistically stationary flows. In the study of Ref. [18], the modified spectrum was assumed to take the form

$$E(\kappa) = E_0(t)\kappa^s H(\kappa_m - \kappa) + C_\kappa \epsilon^{\frac{2}{3}} \kappa^{-\frac{5}{3}} H(\kappa - \kappa_m) \qquad (18)$$

where κ is the wavenumber vector, $E_0(t)$ is a function that becomes a constant in statistically stationary flows, s is an index that can take the value of 2 or 4, C_κ is the Kolmogorov constant, H is a step function, and κ_m denotes the value of κ where the energy-production range is matched to the inertial subrange. By integrating Eq. (18) to obtain k, then by assuming homogeneous isotropic turbulence and after some simplifications, the following equation for the dissipation rate is obtained (see Ref. [18] for details):

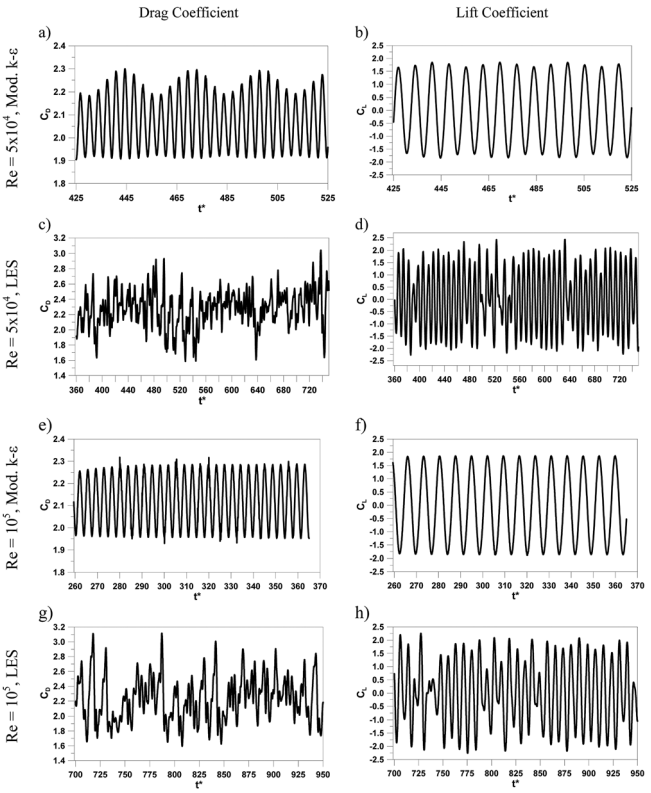

Fig. 5 Predicted C_D (left) and C_L (right) at different Re: (*a*), (*b*) LES (5×10^4); (*c*), (*d*) modified k-ϵ (5×10^4); (*e*), (*f*) LES (10^5); and (*g*), (*h*) modified k-ϵ (10^5)

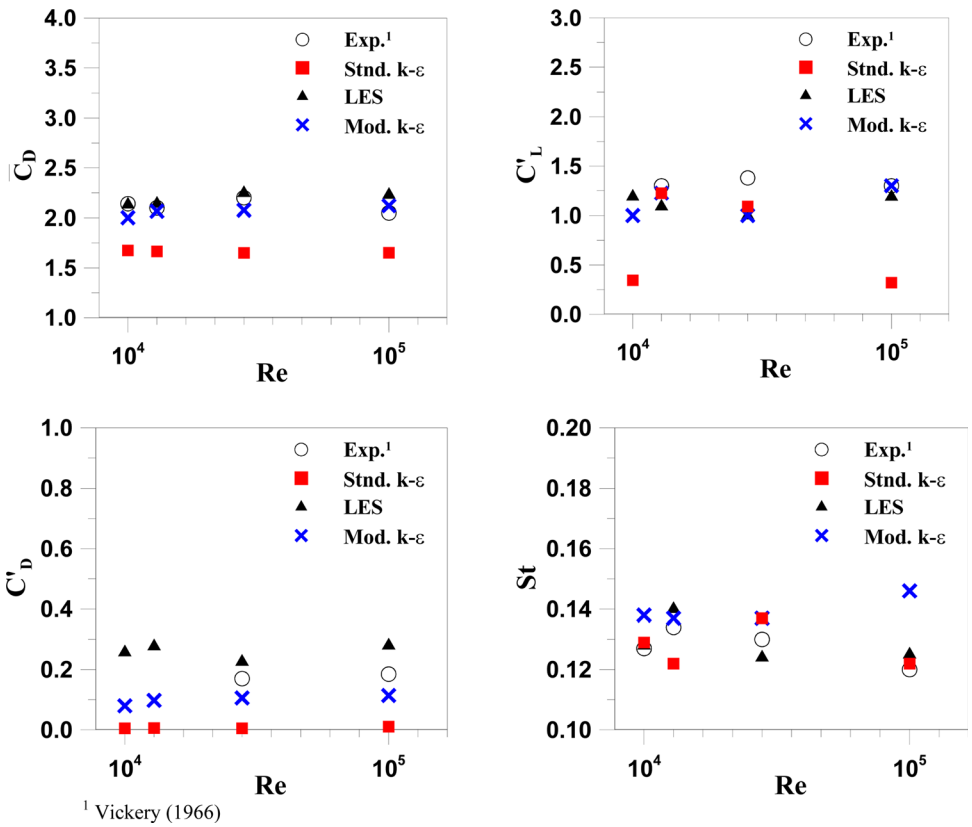

Fig. 4 Predicted and measured variation with Re of the average and rms C_L and C_D and the Strouhal number

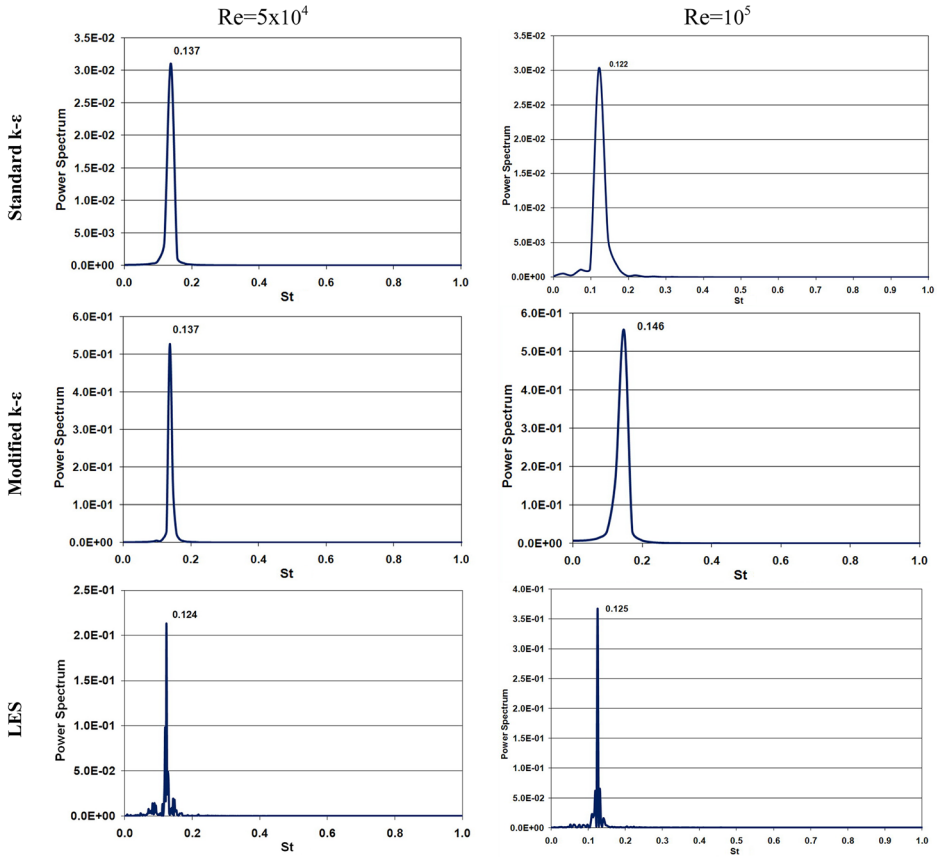

Fig. 6 Energy spectrum for $Re = 5 \times 10^4$ (left) and 10^5 (right). Standard and modified k-ϵ models (top and middle rows), LES (bottom row).

$$\frac{d\epsilon}{dt} = -C_{\epsilon 2}^{0}\frac{\epsilon^2}{k} - \frac{1}{s+1}\frac{\epsilon}{E(\kappa)}\frac{dE(\kappa)}{dt} \tag{19}$$

where $C_{\epsilon 2}^{0} = (3s+5)/2(s+1)$.

From inspection of Eq. (19), it is clear that the ϵ equation should contain a term that explicitly accounts for the modification of the spectral energy transfer process due to the interactions with the mean-flow periodicity and the most direct way for achieving this is to redefine C_{ϵ_1} as

$$C_{\epsilon_1}^{*} = C_{\epsilon_1}\left(1 + C_t\frac{k}{\epsilon}\frac{1}{Q+k}\left|\frac{D(Q+k)}{Dt}\right|\right) \tag{20}$$

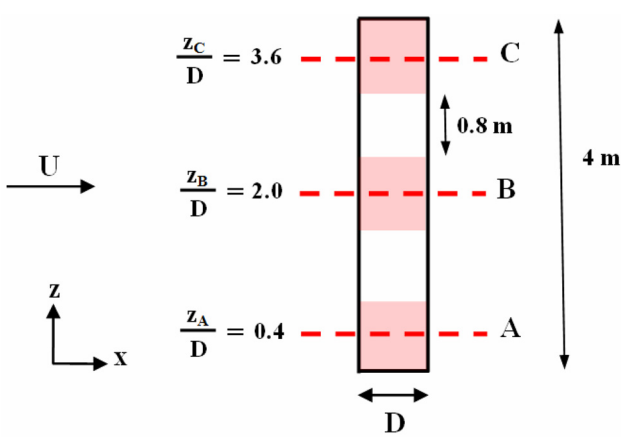

Fig. 7 Vertical section of cylinder showing force monitoring locations A, B, and C

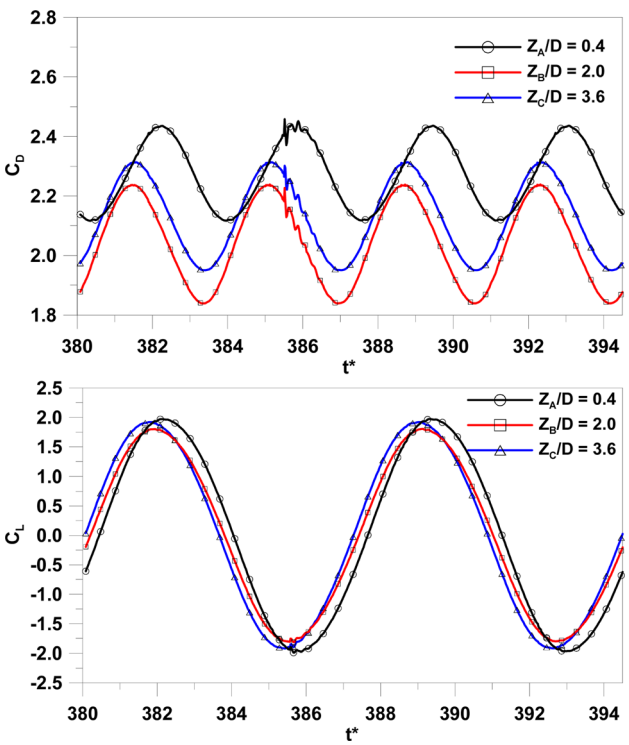

Fig. 8 Drag (top) and lift (bottom) coefficients at monitoring locations. Predictions with modified k-ϵ model ($Re = 10^5$).

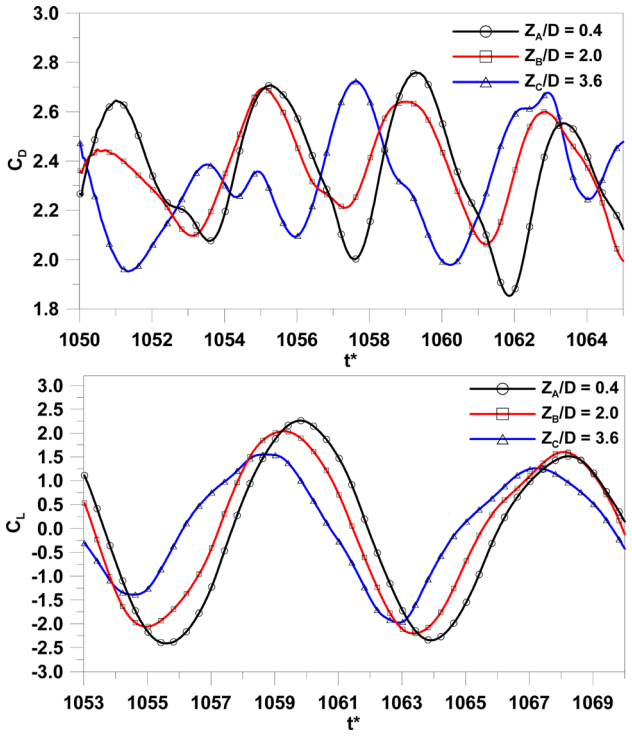

Fig. 9 Drag (top) and lift (bottom) coefficients at monitoring locations. Predictions with LES ($Re = 10^5$).

where q is the mean-flow kinetic energy per unit mass. The coefficient C_t is set equal to 0.38 as in the original reference.

The effectiveness of this modification has already been demonstrated in a number of studies on two-dimensional flows with vortex shedding vortex shedding ([17,20]). The present work extends the verification of this model to three-dimensional flows.

3 Results and Discussion

The governing equations of Sec. 2 were solved using an iterative finite-volume solver. Discretization of the spatial gradients was by third-order accurate bounded scheme while the temporal discretization was by the second-order accurate Crank–Nicholson scheme. The geometry of the square cylinder and the extent of the computational domain are shown in Fig. 1. The square cylinder's cross-sectional dimensions were D ($= 1$ m), and its height was $4D$. The inlet to the computational domain was located at distance $7.5D$ from the upstream face of the cylinder while the outlet was placed at distance of $16D$ from the downstream face. The total width of the domain was set equal to $16D$. The incident flow was aligned with the x-axis. To ensure adequate resolution of the flow, the computational grids used were constructed in a number of separate nonmatching blocks. The grid lines were nonuniformly distributed with the highest concentration of cells being adjacent to the cylinder where the velocity variations were steepest.

To ensure that the results presented are effectively free of numerical discretization errors, grid and time step independence tests were performed for the k-ϵ model. Computations were thus performed on three different grids that consisted of 365,610, 475,294, and 617,882 active cells. The extent of the discretization errors was quantified using the Grid Convergence Index (GCI) method of Celic et al. [21]. The characteristic variable that is required in this method was chosen to be the averaged drag coefficient ($C_D = F_x/(0.5\ \rho\ U_o^2\ A)$, where F_x is the sum of viscous and pressure forces in the x-direction, U_0 is the uniform inlet velocity, and A is the cylinder's projected area). It was found that the nondimensional frequency of vortex shedding (f) expressed as Strouhal number ($St = fD/U_o$) is quite insensitive to grid resolution effects and was, hence, not included in the analysis. The results of these tests are presented in Table 1 where, to maintain the notation

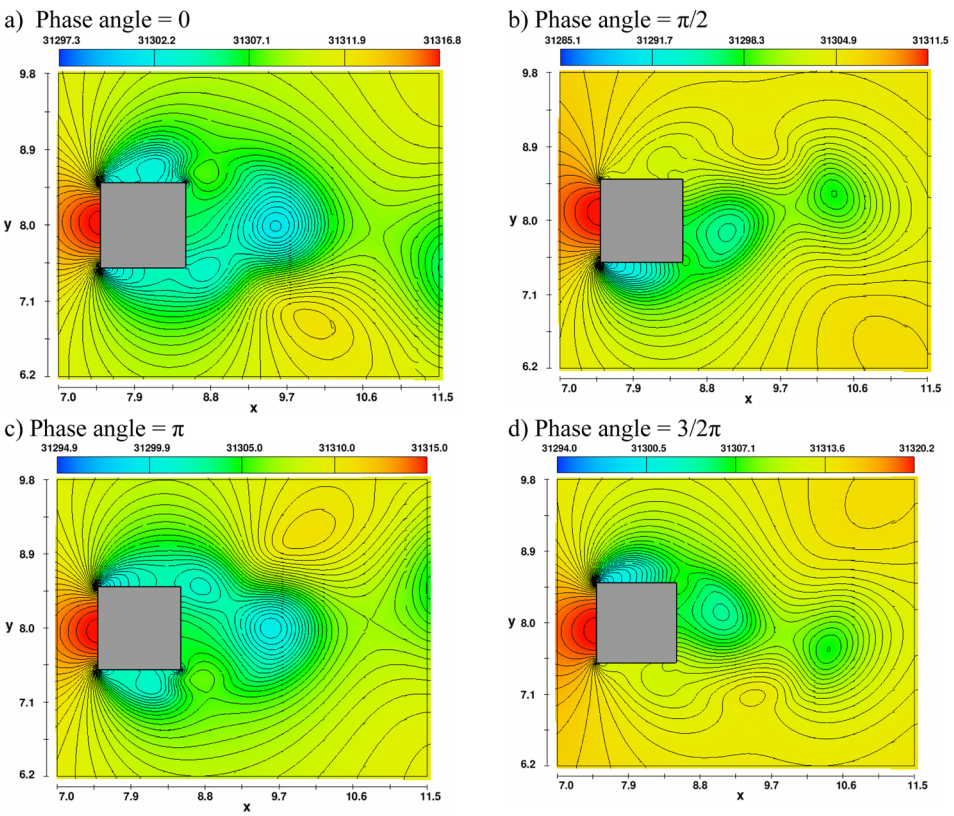

Fig. 10 Modified k-ϵ predictions of the pressure contours (Pa) at different phase angles ($Re = 10^5$)

of Ref. [21], the symbol Φ is used to denote C_D, the characteristic variable. In the table, Φ_{ext}^{21} denotes the extrapolated value of Φ and e_{ext}^{21} is the associated extrapolation error. It is clear from the GCI value of 0.11448% that the results obtained with the grid consisting of 475,294 active cells are sensibly free of grid effects and were hence used in subsequent calculations. This number of cells would not be adequate for the LES computations which, instead, were performed on a grid consisting of a total of 1,453,950 cells (a threefold increase on the URANS grid). With this grid, which is comparable to those used in many previous studies, the cylinder surface at each plane across the principal axis (i.e., in the x-y plane) was resolved with a total of 60 cells. The maximum distance from the cell center to the cylinder's wall ($\Delta h/D$) was set equal to 0.008. Figure 2 shows the multiblock mesh configuration in this plane, containing mesh blocks G, H, I, and J. The cell ratio expansion in the x and y directions was set to 1.24. Thus, for example, mesh block J is expanded from 7.25 m to 8.75 m in the x and y directions, and contains 90 cells in each direction, while mesh block I is expanded from 7 m to 9 m in the x and y directions and contains 108 cells in each direction.

The boundary conditions used in the computations were as follows. At inlet to the computational domain, the streamwise velocity was taken to be uniform across the inlet and was assigned a value according to the desired Reynolds number for the simulations. The y- and z- direction velocity components were set equal to zero. The turbulence kinetic energy was assigned a constant value consistent with a relative turbulent intensity of 1% while the dissipation rate was obtained from inversion of Eq. (14) with the assumption that the ratio of turbulent to molecular viscosity is 10. At the outlet, a nonreflective boundary condition was implemented wherein the streamwise gradients of all dependent variables were set equal to zero. At all remaining boundaries, the normal gradients for all dependent variables were set equal to zero except for the components of velocity normal to these boundaries that were themselves set equal to zero. The cylinder's walls were taken as smooth. In the LES simulations, a no-slip boundary condition was applied at the wall. In the URANS simulations, it was assumed that the flow adjacent to the wall can be described by the standard logarithmic law of the wall thereby allowing for the wall boundary conditions to be specified using the "wall function" approach. While doubts regarding the existence of the log law in separated flows exist, the use of wall functions remains the most frequently used method for specifying the boundary conditions in RANS and URANS. For this reason, it was adopted here in preference to a low Reynolds-number variant of the k-ϵ model. In applying this boundary condition, the center of the cells that are in contact with the cylinder should ideally be located at distance $30 < Y^+ < 50$, i.e., sufficiently removed from the viscous sublayer for the high turbulent Reynolds-number version of the k-ϵ model to be applicable but also sufficiently close to the

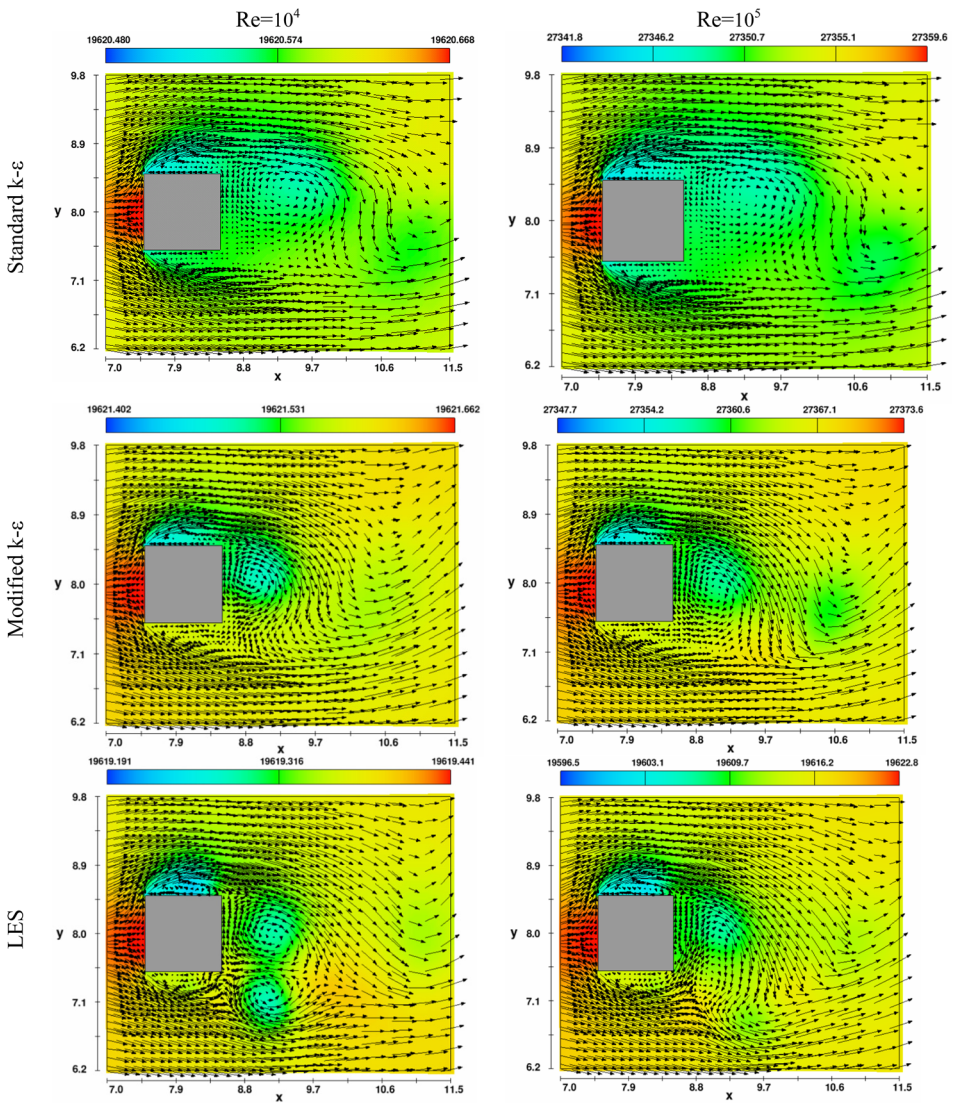

Fig. 11 Predicted velocity vectors (m/s) for $Re = 10^4$ (left column) and 10^5 (right column) with standard and modified k-ϵ models and LES

cylinder walls to be able to capture the small-scale perturbations that originate from there. This is a difficult requirement to achieve in time dependent flows generally, especially those in which large-scale separation is present where the wall shear stress becomes zero at flow reattachment. Nevertheless, and short of adopting a model that can be integrated through the viscous sublayer directly to the wall, a modeling strategy that brings with it a different set of uncertainties, the wall-function approach remains the method of choice in engineering applications even though the limits on Y^+ cannot be strictly enforced at all phases of the shedding cycle.

In presenting the results, we first check that the modification to the k-ϵ model can produce the same degree of improvements in this three-dimensional flow as was previously obtained in the two-dimensional cases. Figure 3 shows the time series for the lift and drag coefficients as predicted first by the standard model and, subsequently, beginning from $t^* = 315$ ($t^* = U_0\, t/D$), with the modification in place. These results are for $Re = 10^5$ ($Re = \rho\, U_0\, D/\mu$). It is clear from this figure that the modification produces significant increase in the mean value of C_D coupled with increases in the strength of fluctuations (in terms of the root mean square) in both the lift and drag coefficients. This response, which is identical to that found in the two-dimensional cases, suggests that the mechanism for interactions between the organized mean-flow periodicity and the random turbulence is equally important here and hence the need for accounting for the effects of vortex shedding on the energy transfer processes in three-dimensional flows as well.

A quantitative assessment of the performance of the modified k-ϵ model and LES is presented in Table 2. For comparison, the results obtained with the standard model are also presented. Listed there are the predicted and measured values of the Strouhal number, the mean drag coefficient, and the root-mean-square values of drag and lift coefficients for Reynolds number of 10^5. Also given in Table 2 are the LES results of Ref. [11] obtained using two different subgrid scale models. The Table also shows the experimental results of Vickery [22]. It is interesting to note that Strouhal number is not particularly sensitive to the choice of simulation approach (LES or URANS) as it can be seen that even the standard k-ϵ model yields a relatively accurate prediction of this parameter while being in serious error in predicting the mean and root-mean-square values. This behavior was previously noted in the prediction of two-dimensional cases as well (e.g., Rodi et al. [23]). Turning to the predicted root-mean-square values of the lift and drag coefficients ($C_L^{'}$ and $C_D^{'}$), the results obtained with the standard model for these two parameters seriously underestimate both the measurements and the range of values obtained with LES and the modified model. In contrast, the present results obtained with LES and the modified k-ϵ model are in quite close agreement with the data of Ref. [22]. The modified model's result for C_D is particularly close, being within 3.4% of the data. The same model appears to underpredict $C_D^{'}$ relative to the LES result. Both the modified model and the LES results for $C_L^{'}$ are in close accord with the data.

To explore the dependence of the models performance on Reynolds number, predictions with the LES and both the standard and the modified k-ϵ models of mean and fluctuating force coefficients and of Strouhal number are presented in Fig. 4 for values of Reynolds number in the range $10^4 < Re < 10^5$. Also plotted there are the data of Ref. [22]. The predicted time series of the lift and drag coefficients for $Re = 5 \times 10^4$ and 10^5 are presented in Fig. 5. The behavior seen there is quite complex where it is clear that the fluctuations in the lift and drag coefficients occur over a range of frequencies the dominant one being the frequency of vortex shedding. In contrast to the LES results, the URANS results do not capture the small-scale high-frequency oscillations in lift and drag, returning instead a quasi-periodic behavior. This is due to the use of wall functions to determine the wall boundary conditions: matching the computed solutions to the log-law means that the near-wall region, where the small-scale fluctuations will have originated from, would not be properly resolved. Figure 6 presents the energy spectra obtained by performing fast Fourier transform analysis on the time series of the lift and drag coefficients presented in Fig. 5. Note the close correspondence between the various models predictions of the dominant (Strouhal) frequency, and note also that the peak energy predicted by the standard k-ϵ model is one order of magnitude smaller than the results of both the modified model and the LES.

To illustrate the models' performance in capturing the expected three-dimensional behavior of this flow, the predicted time series of

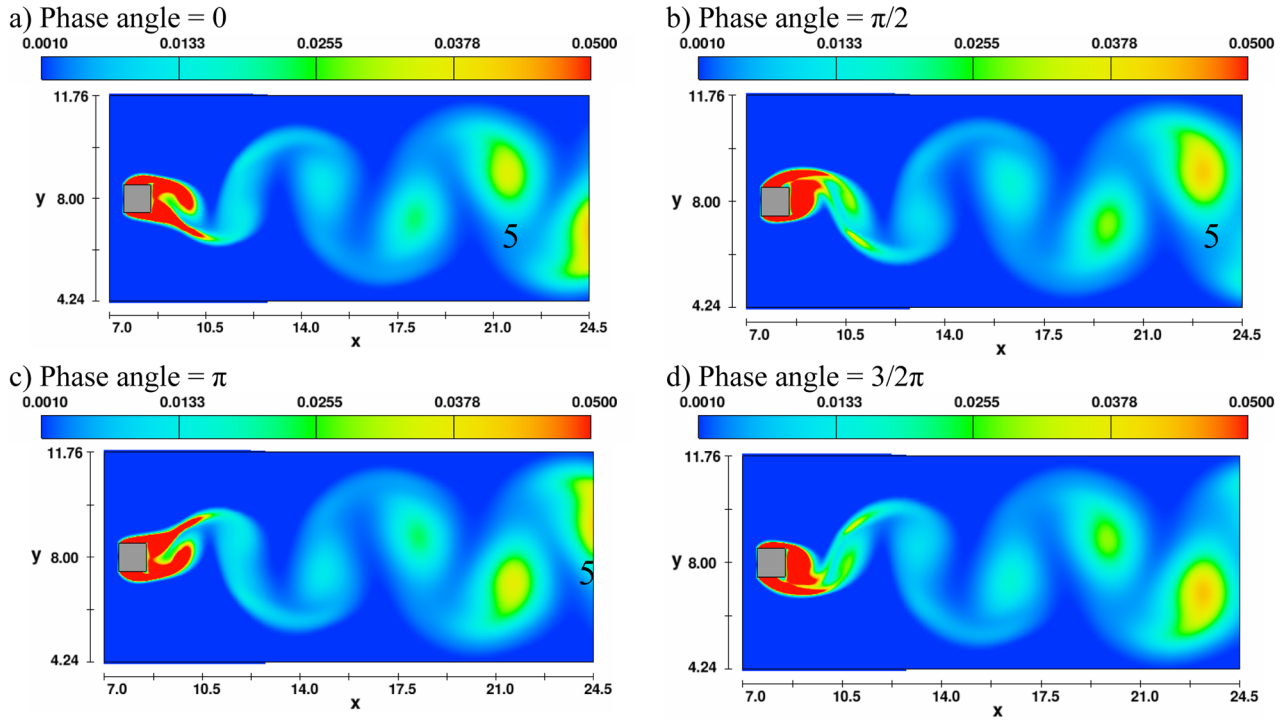

Fig. 12 Dependence of eddy viscosity on phase angle as predicted with the modified k-ϵ model. Results shown are at $z/D = 1.8$ ($Re = 10^5$).

the local values of C_D and C_L at different heights from the base of the cylinder are examined. To this end, the cylinder's height (4 m) is divided into five equal sections as shown in Fig. 7, and the time series of C_D and C_L were obtained from the simulations for sections A, B, and C. The heights of these sections relative to the base, nondimensionalized by the cylinder width, are 0.4, 2.0, and 3.6, respectively. The predicted values of C_D and C_L obtained with the modified model are shown in Fig. 8. As can be seen there, the variation of the drag and lift coefficients with time occur at significantly different phases depending on location along the cylinder's axis. This is consistent with there being significant three-dimensional effects as observed in experiments. The corresponding LES results are shown in Fig. 9. Here, too, the three-dimensional behavior is very apparent as evidenced by the time lag in the occurrence of the peak values in C_D and C_L. These results confirm the ability of both models to capture the three-dimensional nature of vortex shedding at Reynolds number of 10^5.

The predicted contours of pressure around the cylinder are shown in Fig. 10. The phases indicated on the plots refer to the C_L cycle with the phase angle being 0 when $C_L = 0$. As shown in this figure, the flow close to the upper right corner of the cylinder ($x = 8.5$ m, and $y = 8.5$ m) has higher pressure compare to the neighboring flow at the lower right corner of the cylinder ($x = 8.5$ m, and $y = 7.5$ m), which the fluid in a zone with higher pressure displaces towards the opposite corner while getting far from the cylinder as shown in Fig. 10(*b*), representing phase angle $\pi/2$; then a high pressure generates at the upper side of the depicted cylinder plane, causing a very high lift force on the cylinder. While the vortex is being convected away from the cylinder, a higher pressure forms close to the lower left corner of the cylinder ($x = 7.5$ m, and $y = 7.5$ m), which the upper and lower side pressures on the cylinder are minimum, causing the minimum lift force on the cylinder at phase angle π. Finally, the newly generated vortex leaves the area close to the cylinder's corner, and a high pressure generates on the lower side of the cylinder causing another high lift force on the structure. Figure 10(*d*) shows this phase (i.e., phase 3/2 π) depicting the cross section of the new vortex at about $x = 9.1$ m, while the old vortex is at about $x = 10.4$ m at this phase angle. The formation of the vortices at higher and lower pressures at different phases at the wake of the square cylinder causing high and low lift forces on the square cylinder were presented in this section from the predictions by the modified k-ϵ model. These results are in agreement with other computational predictions such as the ones reported in [12,17].

The computed flow field in the wake of a square cylinder for $Re = 10^4$ and 10^5 are shown in Fig. 11. These results were obtained with the standard and modified k-ϵ models and LES at the phase of a vortex shedding cycle where C_L is minimum (i.e., phase angle = 0). In all of the mentioned scenarios, the velocity vectors show delayed separation for the standard k-ϵ model's predictions as can be seen in top rows of the these figures compared to the middle and bottom rows, which represent the modified k-ϵ model and LES results, respectively. Another conclusion from these figures is that the generated vortices by using the standard k-ϵ model were not accurately predicted as the ones predicted by the other two models. This failure can also be concluded from the

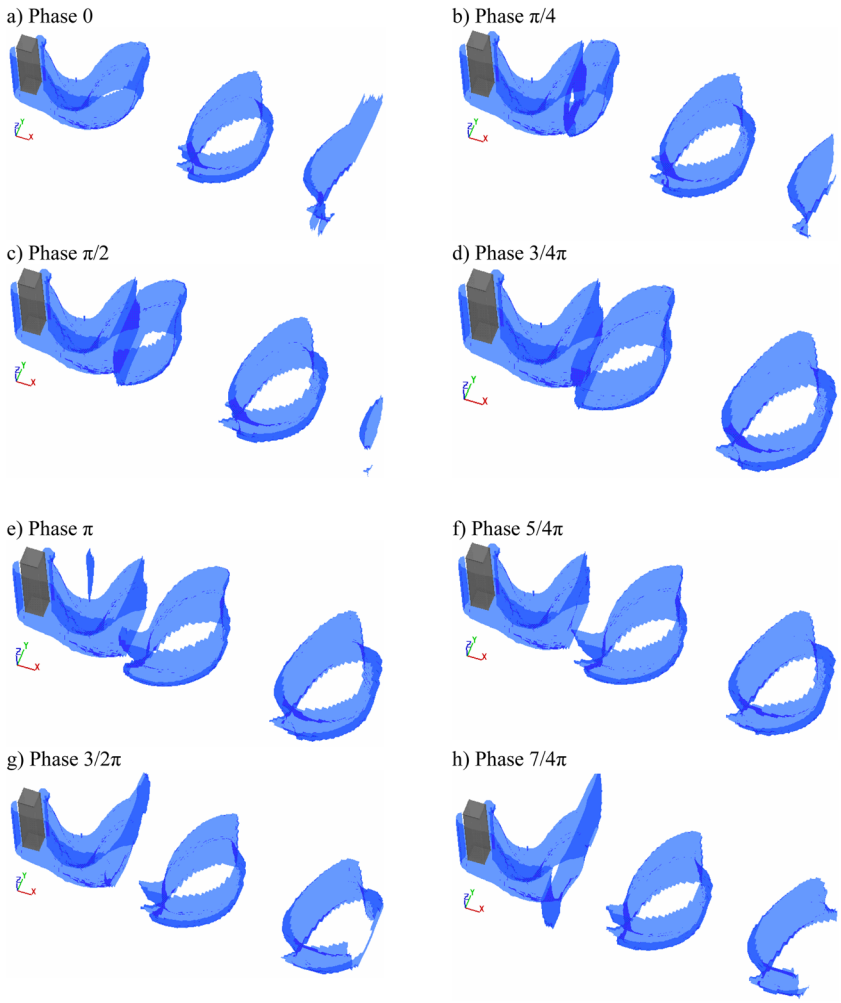

Fig. 13 Modified k-ϵ model results for the vertical component of vorticity ($Re = 10^5$)

Fig. 6 where the power spectrum of the dominant Strouhal number was about 10 times smaller for the standard k-ϵ model's results compared to the rest. These are due to the fact that the two equation k-ϵ model in the standard form fails to correctly predict the vortex generation and shedding phenomenon for flows with high Reynolds numbers in the wake of a cylinder where large scale mean-flow periodicity is an important feature.

It should also be noted that the predicted flow field in the wake of the cylinder obtained with LES and the modified k-ϵ model had shown some differences, e.g., where the LES predicted some smaller vortices in the wake of the cylinder in addition to the dominant vortex, while the modified k-ϵ predicts a single dominant vortex in the wake of the cylinder as shown in Fig. 11. This phenomenon is also apparent in Fig. 6, where the LES predictions showed the presence of additional spikes around the dominant Strouhal number that are not apparent in the modified k-ϵ model results.

As the predictions of the modified model are largely determined by its ability to produce the correct levels of turbulent viscosity in the field, it is instructive to see how this parameter varies with time at a particular cross section along the cylinder's axis. The section chosen is at distance $z/D = 1.8$, and the contours of turbulent viscosity are plotted in Fig. 12. It is immediately apparent that the modified k-ϵ model does not produce regions of excessively high eddy viscosity around the stagnation point. The presence of this region, which is attributed to excessive production of turbulence kinetic energy by normal strains, has previously been cited as the reason for the inability of the standard model to produce the correct strength of vortex shedding. This is clearly not obtained in the modified closure.

Isosurfaces of the vertical component of the vorticity are shown at different phases in Fig. 13. By following the phases from 0 to 7/4 π, the generation and propagation of vortices are shown for one C_L cycle. Phases 0 and π correspond with the time when lift force on the cylinder is zero, and phases $\pi/2$ and $3/2\ \pi$ correspond with the condition where the lift force is maximum. As can be seen in these figures, the vorticity distribution varies considerably in the vertical direction. This is an indication of the existence of three-dimensional vortices in the wake of the cylinder that stretch nonuniformly. The formation of vortices in the wake of a circular cylinder was examined by Xu and Dalton [24] using LES with results that are quite similar to those obtained here.

4 Conclusions

In this study, we report on the prediction of the unsteady flow field around, and the resulting forces on a three-dimensional surface-mounted square cylinder at Reynolds numbers in the range 10^4–10^5. The unknown correlations that arise from averaging the equations governing the instantaneous flow field were determined using two alternative approaches: LES and URANS. The main contribution of this work has been the finding that the use of URANS can produce predictions that are in the main similar to those obtained with LES provided that the consequences of the interactions between the large-scale organized mean-flow periodicity and the small-scale random turbulence motions are properly accounted for in the URANS formulation. A modification to the standard k-ϵ that has been extensively validated in two-dimensional flows was shown to successfully capture the effects of these interactions in the three-dimensional flow as well. Thus, the widely-held view (e.g., Castro and Graham [25]) that the standard turbulence models used in computational fluid dynamics are seriously inadequate for studying flow around bluff bodies is confirmed here by our results with the standard k-ϵ model. However, the suggestion that only by using LES can the effects of turbulent vortex shedding be accurately predicted is not one supported by the present results. The results presented here and elsewhere (e.g., Ref. [26].) clearly demonstrate that by appropriately accounting for the effects of organized mean-flow unsteadiness on the turbulence, URANS can yield results that are on par with LES but at significantly lower costs in terms of computer resources.

Acknowledgment

BAY wishes to record his profound gratitude to Professor M. Y. Hussaini who, as Director of ICASE, facilitated most fruitful interactions with the ICASE resident scientists. It was through one of these interactions that the mathematical basis of the turbulence-model modification presented in this paper was formalized.

References

[1] Blevins, R. D., 2009, "Models for Vortex-Induced Vibration of Cylinders Based on Measured Forces," ASME J. Fluids Eng., **131**(10), p 101203.
[2] Mahir, N., 2009, "Three-Dimensional Flow Around a Square Cylinder Near a Wall," Ocean Eng., **36**(5), pp. 357–367.
[3] Ozkol, U., Wark, C., and Fabris, D., 2007, "Mean and Fluctuating Velocity Characteristics of a Separated Shear Layer Past a Surface Mounted Block," ASME J. Fluids Eng., **129**(2), pp. 200–209.
[4] Pope, S. B., 2000, *Turbulent Flows*, Cambridge University Press, Cambridge, UK.
[5] Lim, H. C., Thomas, T. G., and Castro, I. P., 2009. "Flow Around a Cube in a Turbulent Boundary Layer: LES and Experiment," J. Wind Eng. Ind. Aerodyn., **97**(2), pp. 96–109.
[6] Hussein, H. J., and Martinuzzi, R. J., 1996, "Energy Balance for Turbulent Flow Around a Surface Mounted Cube Placed in a Channel," Phys. Fluids, **8**(3), pp. 764–780.
[7] Srinivas, Y., Biswas, G., Parihar, A. S., and Ranjan, R., 2006, "Large-Eddy Simulation of High Reynolds Number Turbulent Flow Past a Square Cylinder," J. Eng. Mech., **132**(3), pp. 327–335.
[8] Kim, Y., and Kanda, J., 2010, "Characteristics of Aerodynamic Forces and Pressures on Square Plan Buildings With Height Variation," J. Wind Eng. Ind. Aerodyn., **98**(8–9), pp. 449–465.
[9] Bruno, L., Fransos, D., Coste, N., and Bosco, A., 2011, "3D Flow Around a Rectangular Cylinder: A Computational Study," J. Wind Eng. Ind. Aerodyn., **98**(6–7), pp. 263–276.
[10] Pope, S. B., 2004, "Ten Questions Concerning the Large-Eddy Simulation of Turbulent Flows," New J. Phys., **6**(3), pp. 1–24.
[11] Krajnovic, S., and Davidson, L., 2002, "Large-Eddy Simulation of the Flow Around a Bluff Body," AIAA J., **40**(5), pp. 927–936.
[12] Sohankar, A., 2006, "Flow Over a Bluff Body From Moderate to High Reynolds Numbers Using Large Eddy Simulation," Comput. Fluid., **35**(10), pp. 1154–1168.
[13] Oka, S. and Ishihara, T., 2009, "Numerical Study of Aerodynamic Characteristics of a Square Prism in Uniform Flow," J. Wind Eng. Ind. Aerodyn., **97**(11–12), pp. 548–559.
[14] Ramesh, V., Vengadesan, S., and Narasimhan, J. L., 2006, "3D Unsteady RANS Simulation of Turbulent Flow Over Bluff Body by Non-Linear Model," Int. J. Num. Meth. Heat Fluid Flow, **16**(6), pp. 660–673.
[15] Smith, H. D., and Foster D. L., 2005, "Modeling of Flow Around a Cylinder Over a Scoured Bed," J. Waterway Port Coast Ocean Eng., **131**(1), pp. 14–24.
[16] Bosch, G., and Rodi, W., 1998, "Simulation of Vortex Shedding Past a Square Cylinder With Different Turbulence Models," Int. J. Num. Meth. Fluids, **28**(4), pp. 601–616.
[17] Younis, B. A., and Przulj, V. P., 2006, "Computation of Turbulent Vortex Shedding," Computat. Mech., **37**(5), pp. 408–425.
[18] Younis, B. A., and Zhou, Y., 2006, "Accounting for Mean-Flow Periodicity in Turbulence Closures," Phys. Fluids, **18**(1), p. 018102.
[19] Durao, D., Heitor, M., and Pereira, J., 1988, "Measurements of Turbulent and Periodic Flows Around a Square Cross-Section Cylinder," Experiment. Fluids, **6**(5), pp. 298–304.
[20] Przulj, V. P., 1998, "Computational Modelling of Vortex Shedding Flows" Ph.D. thesis, City University, London.
[21] Celik, I. B., Ghia, U., Roache, P. J., Freitas, C. J., Coleman, H., and Raad, P. E., 2008, "Procedure for Estimating and Reporting of Uncertainty Due to Discretization in CFD Applications," ASME J. Fluids Eng., **130**(7), p. 078001.
[22] Vickery, B. J., 1966, "Fluctuating Lift and Drag on a Long Cylinder of Square Cross-Section in a Turbulent Stream," J. Fluid Mech., **25**(3), pp. 481–494.
[23] Rodi, W., Ferziger, J. H., Breuer, M., and Pourquie, M., 1997, "Status of Large Eddy Simulation: Results of a Workshop," ASME J. Fluids Eng., **119**(2), pp. 248–262.
[24] Xu, Y., and Dalton, C., 2001, "Computation of Force on a Cylinder in a Shear Flow," J. Fluids Struct., **15**(7), pp. 941–954.
[25] Castro, I. P., and Graham, J. M. R., 1999, "Computational Wind Engineering: The Way Ahead?," Proc. Inst. Civil Eng. Struct., **134**(3), pp. 275–277.
[26] Abrishamchi, A., and Younis, B. A., 2012, "LES and URANS Predictions of the Hydrodynamic Loads on a Tension-Leg Platform," J. Fluids Struct., **28**(1), pp. 244–262.